IEEE Access
Multidisciplinary ⋮ Rapid Review ⋮ Open Access Journal

Received 4 October 2023, accepted 8 November 2023, date of publication 14 November 2023,
date of current version 22 November 2023.

Digital Object Identifier 10.1109/ACCESS.2023.3332758

RESEARCH ARTICLE

High-Performance Permanent Magnet Synchronous Motor Control With Electrical Angle Delayed Component Compensation

SEONHYEONG KIM[1], KEUNHO PARK[2], DONGKIL KANG[1], AND GEUN HO LEE[1]
[1]Department of Automotive Engineering, Kookmin University, Seongbuk-gu, Seoul 02707, South Korea
[2]Korea Institute of Electronics Technology, Jeonju-si, Jeollabuk-do 54853, South Korea

Corresponding author: Geun Ho Lee (motor@kookmin.ac.kr)

This work was supported by the Korea Institute of Planning and Evaluation for Technology in Food, Agriculture and Forestry (IPET) through the Open Field Smart Agriculture Technology Short-Term Advancement Program funded by the Ministry of Agriculture, Food and Rural Affairs (MAFRA) under Grant 322030031HD030.

ABSTRACT Electrical angle delay resulting from inverter part and design errors causes rotor position errors. It significantly lowers motor control performance as the rotor position error rate increases owing to increased speed. Rotor position detections considering the delay component can be classified into initial rotor-position and time-delay position detections. The initial rotor position detection method causes initial rotor position errors based on speed because it does not consider the electrical angle delay component. The conventional time-delay position detection method involves current–voltage time-delay position detection. The dynamo system manually measures and compensates for current and voltage delay coefficients based on speed to detect the time-delay position. However, achieving precise torque control performance is challenging because detecting the delay coefficient at high speeds is dangerous, and separating the electrical angle delay component is impossible. This study proposes a delay component detection and compensation algorithm by analyzing the electrical angle delay component due to inverter parts and design errors. The new initial rotor and time-delay positions are estimated to improve the torque control performance by compensating for the detected delay component. The proposed algorithm is based on the PMSM voltage equation and validated through simulation using MATLAB Simulink. The initial rotor position, time-delay position, and torque control performance are verified by experimentally detecting and compensating for the electrical angle delay component using the proposed algorithm. The results demonstrate that the proposed algorithm is robust to inverter part and design errors. Moreover, the proposed algorithm is advantageous in considerably improving the torque control performance.

INDEX TERMS Current time delay, delayed components, electrical angle, electrical angle offset, initial rotor position, permanent magnet synchronous motor, time-delay position, torque control, voltage time delay.

I. INTRODUCTION

Recently, permanent magnet synchronous motors (PMSMs) have been widely adopted in mobile bodies, automobiles, agricultural machinery, and urban air mobility (UAM) fields owing to their high-power density advantages. In line with this trend, precise high-speed control of PMSMs is necessary for miniaturization and high efficiency. High-speed control of PMSM requires accurate rotor positioning and d-q axis vector control in the rotor position-aligned synchronous rotating frame [1], [2], [3], [4], [5], [6], [7].

Typically, position sensors, such as resolvers, encoders, Hall sensors, and magnetoresistive (MR) sensors, are used to accurately detect rotor position. However, to design for rotor position detection, different circuit designs are required owing to type of sensors and filter time constants

The associate editor coordinating the review of this manuscript and approving it for publication was Francisco Perez-Pinal.

(caused by noise), which lead to design errors [8], [9], [10], [11], [12], [13].

Resolvers have hardware delayed components, such as filter and integrated circuit (IC) delays for excitation, sin, and cos signals, whereas encoders experience hardware delays, such as sensor and filter delays for A/B signals. Moreover, software processing the position information has peripheral delays owing to clock frequency and interrupt timing. Delays also occur when converting a position sensor signal into a rotor position using an algorithm, thus leading to position information errors. Each position delay causes errors depending on the design, and the delayed component cannot be easily measured. In addition, electrical angle errors increase with increasing drive frequency owing to error components, thus deteriorating PMSM control performance at high speeds. Specifically, a maximum speed of approximately 500 Hz is necessary in electric vehicle systems to achieve miniaturization and a high-efficiency drive motor [14], [15] Therefore, delayed components must be identified and compensated for secure precise torque control and performance in the weak magnetic flux region [16], [17].

Rotor position detection can be classified into initial and time-delay, as shown in Fig. 1.

Existing methods of detecting initial rotor position include the unidirectional drive based on the d-q axis voltage equation, high-frequency injection, and d-axis alignment methods [18], [19], [20], [21], [22], [23], [24].

The unidirectional drive method is advantageous owing to its ease of algorithm implementation. However, it includes delayed components varying with the measurement speed, thereby resulting in errors in the initial rotor position at different speeds.

The high-frequency injection method can accurately detect the initial position by calculating the inductance at rest. However, it cannot easily implement and test the algorithm owing to the signal processing required by high-frequency injection, particularly in cases with low saliency ratios.

The d-axis alignment method, which relies solely on d-axis current control for initial position detection, can detect the initial position but produces vibrations caused by motor inertia during d-axis alignment, thus leading to errors in the initial position owing to the influence of current control performance.

Time-delay position detection methods can be categorized into position, current, and voltage time-delay compensations. However, studies have focused primarily on current time-delay compensation, where a manual speed-specific d-axis current is applied to the dynamo system, and delay coefficients are detected to compensate for the 0-Nm torque generation. Moreover, voltage time-delay compensation has been achieved by increasing the speed while controlling the d-q axis current to 0 A and ensuring no d-axis voltage is generated or compensating for $1.5t_s$ [25], [26]. However, such methods are inapplicable for detecting delay coefficients at high speeds and cannot distinguish and detect the electrical angle delayed component, essentially limiting their ability to ensure precise torque control performance.

Therefore, this study measured hardware and software delayed components and analyzed them through a delayed component detection algorithm using the d-q axis voltage equation. Furthermore, torque control performance at high speeds was verified through compensation for the electrical angle delayed components. This delayed component compensation method can be applied to various types of position sensors, and applies to motor performance verification and mass production.

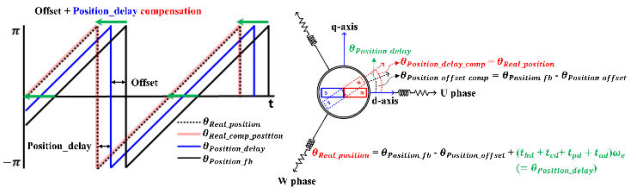

FIGURE 1. Electrical angle and d-q axis rotor position according to delayed components.

II. ROTOR POSITION DETECTION WITH ELECTRICAL ANGLE DELAYED COMPONENT COMPENSATION

A. ROTOR POSITION DETECTION WITH THE GENERAL METHOD

The unidirectional drive method, a simple algorithm that enables initial position estimation and is primarily used in mass production, was researched as a preliminary study. The unidirectional drive method uses a dynamo system to control the PMSM speed. The initial rotor position is calculated using (1) and (2) based on the d-q axis voltage of the PMSM synchronous coordinate system.

$$V_d = (L_1 - L_2 \cos 2\theta_o)\frac{di_d}{dt} - L_2 \sin 2\theta_o \frac{di_q}{dt} - \omega_e \phi_f \sin\theta_o + i_d (R_s + L_2 \omega_e \sin 2\theta_o) - i_q \omega_r (L_1 + L_2 \cos 2\theta_o), \tag{1}$$

$$V_q = (L_1 + L_2 \cos 2\theta_o)\frac{di_q}{dt} - L_2 \sin 2\theta_o \frac{di_d}{dt} + \omega_e \phi_f \cos\theta_o + i_q (R_s - L_2 \omega_e \sin 2\theta_o) - i_d \omega_r (L_1 - L_2 \cos 2\theta_o), \tag{2}$$

where $V_d, V_q, i_d,$ and i_q represent the voltage and current of the d-q axis of the synchronous coordinate system; $L_1, L_2, R_s, \omega_e,$ and ϕ_f are the inductance ($L_d = (L_1 - L_2), L_q = L_1 + L_2$), resistance, rotor speed, and magnetic flux, respectively; and θ_o represents the initial rotor position error.

When the d-q axis current is in a steady-state and controlled to 0 A, it can be represented using (3)–(6).

$$V_d^{ccw} = -\omega_e^{ccw} \phi_f \sin\theta_o, \tag{3}$$

$$V_q^{ccw} = \omega_e^{ccw} \phi_f \cos\theta_o, \tag{4}$$

$$V_d^{cw} = -\omega_e^{cw}\phi_f \sin\theta_o, \tag{5}$$
$$V_q^{cw} = \omega_e^{cw}\phi_f \cos\theta_o, \tag{6}$$

where V_d^{ccw} and V_q^{ccw} represent the d-q axis voltage when rotating counterclockwise at ω_e^{ccw} speed; and V_d^{cw} and V_q^{cw} represent the d-q axis voltage when rotating clockwise at ω_e^{cw} speed. The initial rotor position can be represented using (7).

$$\theta_o = \tan^{-1}\left(\frac{V_d^{ccw}}{V_q^{ccw}}\right) = \tan^{-1}\left(\frac{V_d^{cw}}{V_q^{cw}}\right) \tag{7}$$

Moreover, the time-delay position detection method can be represented by the current and voltage delay detection methods using (8) and (9).

$$\theta_{Current\_delay} = \theta_{Position\_fb} - \theta_o + \alpha_{Current\_Coeff} t_s \omega_e, \tag{8}$$

where $\theta_{Position\_fb}$ is the rotor position read from the position sensor; and $\alpha_{current\_Coeff}$ is a delay coefficient that includes current and position delays, which can lead to errors because it cannot differentiate between position delayed components.

$$\theta_{Voltage\_delay} = \theta_{Position\_fb} - \theta_o + \alpha_{voltage\_Coeff} t_s \omega_e, \tag{9}$$

where $\alpha_{voltage\_Coeff}$ is a coefficient that includes voltage and position delays. Generally, a voltage delay coefficient of 1.5 is used; however, it can lead to errors because it cannot differentiate between position delayed components.

B. ROTOR POSITION DETECTION WITH DELAYED COMPONENT DETECTION AND COMPENSATION

Electrical angle delayed components can be divided into hardware and software delayed components. Therefore, the delayed component (φ_d) can be expressed using (10):

$$\begin{aligned}\varphi_d &= \varphi_{hd} + \varphi_{cd} + \varphi_{pd} + \varphi_{ad} \\ &= (t_{hd} + t_{cd} + t_{pd} + t_{ad})\omega_e = t_d\omega_e,\end{aligned} \tag{10}$$

where φ_{hd} represents difficult-to-measure delayed components, such as those from the position sensor and IC devices; and φ_{cd} represents circuit filter delayed components, both of which are hardware delayed components. For software delayed components, φ_{pd} and φ_{ad} represent peripheral and algorithm delayed components, respectively. The d-q axis voltage equation, which includes the delayed components, can be expressed using (11) and (12), as shown in the phasor diagram in Fig. 2.

$$\begin{aligned}V_d = {} & (L_1 - L_2\cos 2(\theta_o + \varphi_d))\frac{di_d}{dt} \\ & - L_2 \sin 2(\theta_o + \varphi_d)\frac{di_q}{dt} - \omega_e\phi_f \sin(\theta_o + \varphi_d) \\ & + i_d(R_s + L_2\omega_e \sin 2(\theta_o + \varphi_d)) \\ & - i_q\omega_e(L_1 + L_2\cos 2(\theta_o + \varphi_d))\end{aligned} \tag{11}$$

$$\begin{aligned}V_q = {} & (L_1 + L_2\cos 2(\theta_o + \varphi_d))\frac{di_q}{dt} \\ & - L_2 \sin 2(\theta_o + \varphi_d)\frac{di_d}{dt} + \omega_e\phi_f \cos(\theta_o + \varphi_d) \\ & + i_q(R_s - L_2\omega_e \sin 2(\theta_o + \varphi_d))\end{aligned}$$

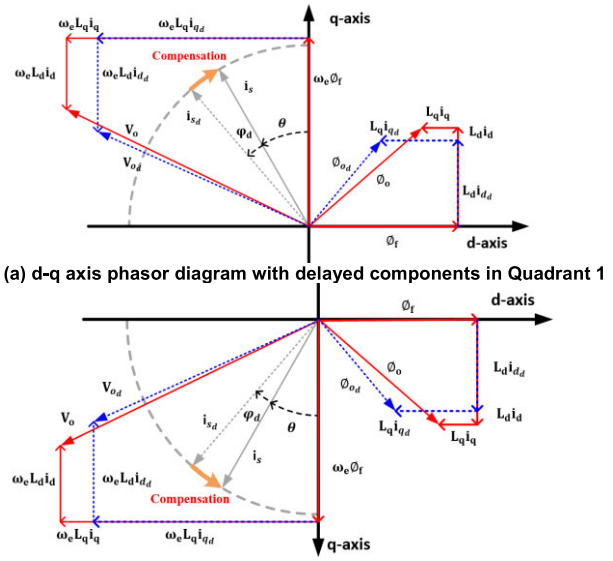

FIGURE 2. d-q axis phasor diagram with delayed components.

$$- i_d\omega_e(L_1 - L_2\cos 2(\theta_o + \varphi_d)) \tag{12}$$

When the d- and q-axis currents are at steady-states and controlled to 0 A, they can be expressed using (13) and (14).

$$\begin{aligned}V_d &= -\omega_e\phi_f \sin(\theta_o + \varphi_d) \\ &= -\omega_e\phi_f \sin(\theta_o + t_d\omega_e),\end{aligned} \tag{13}$$
$$\begin{aligned}V_q &= \omega_e\phi_f \cos(\theta_o + \varphi_d) \\ &= \omega_e\phi_f \cos(\theta_o + t_d\omega_e),\end{aligned} \tag{14}$$

where θ_o represents the initial position error between the position sensor and U phase; and $t_d\omega_e$ represents the position error due to delayed components. The rotor position detection equation that includes delayed components can be represented using (15) and (16).

$$\begin{aligned}\theta^{ccw} &= \text{atan}\left(\frac{V_d^{ccw}}{V_q^{ccw}}\right), \\ &= \theta_o + t_d|\omega_e|\end{aligned} \tag{15}$$
$$\begin{aligned}\theta^{cw} &= \text{atan}\left(\frac{V_d^{cw}}{V_q^{cw}}\right), \\ &= \theta_o - t_d|\omega_e|\end{aligned} \tag{16}$$

where θ^{ccw} and θ^{cw} represent the rotor position errors during forward and reverse rotations, respectively. The delayed component detection (17) and (18), and initial rotor position detection (19) and (20) can be derived using the difference between (15) and (16).

$$\Delta\theta = 2t_d|\omega_e| \tag{17}$$
$$t_d = \frac{\Delta\theta}{2|\omega_e|} \tag{18}$$
$$\theta_o = \theta^{ccw} - \frac{\Delta\theta}{2} \tag{19}$$
$$\theta_o = \theta^{cw} + \frac{\Delta\theta}{2} \tag{20}$$

$\Delta\theta(\theta^{ccw} - \theta^{cw})$ represents the difference between the rotor position during forward and reverse rotation and can detect the delayed component t_d.

C. ROTOR TIME-DELAY POSITION DETECTION WITH DELAYED COMPONENT COMPENSATION

As shown in Fig. 5, the time-delay position through the delayed component (t_d) compensation can be represented as position, current, and voltage time-delay compensations. Therefore, the position time-delay compensation equation can be represented using (21).

$$\theta_{Position\_delay\_comp} = \theta_{Position\_fb} - \theta_o + t_d\omega_e, \tag{21}$$

where $\theta_{Position\_delay\_comp}$ can be represented by $\theta_{Position\_fb}$, read from the position sensor, initial rotor position θ_o with delayed component compensation, and position time delay $t_d\omega_e$. The current time-delay compensation with position time-delay compensation can be represented using (22).

$$\theta_{Current\_delay\_comp} = \theta_{Position\_fb} - \theta_o + t_d\omega_e + \alpha_{Current\_Coeff}\, t_s\omega_e, \tag{22}$$

where $\theta_{Current\_delay\_comp}$ represents the rotor position with delayed component compensation in the current synchronous rotating frame. It can distinguish between the electrical angle delay and current delayed components. As shown in Fig. 3(a), $\alpha_{Current\_Coeff}\, t_s$ represents the current delayed component, which includes current sensor output delay, filter delay, and delay at the point of reading the current. The current delayed component is minimized in the design because current delay affects the current size.

$$\theta_{Voltage\_delay\_comp} = \theta_{Position\_fb} - \theta_o + t_d\omega_e + (1.0t_{s(n)} + 0.5t_{s(n+1)})\omega_e, \tag{23}$$

where $\theta_{Voltage\_delay\_comp}$ represents the rotor position with delayed component compensation in the voltage-synchronous rotating frame. It can distinguish between the electrical angle delay and voltage delayed components. The voltage delayed component, as shown in Fig. 3(b), is compensated by $1.0t_{s(n)}$ owing to the reflection of the pulse width modulation (PWM) next cycle and by $0.5t_{s(n+1)}$ owing to the average voltage of the next cycle.

The electrical angle is subject to an increasing error with increased driving frequency owing to various delayed components. These errors result in inaccuracies in the rotor position during the current and voltage coordinate transformation processes. Consequently, the current sensing timing and voltage vector command are delayed, reducing the vector control performance. Fig. 4 compares the rotor position before and after delayed component compensation at high speeds, thus revealing large errors. As shown in Fig. 5, the system detects position delayed components and improves high-speed torque control performance through position, current, and voltage time-delay compensations.

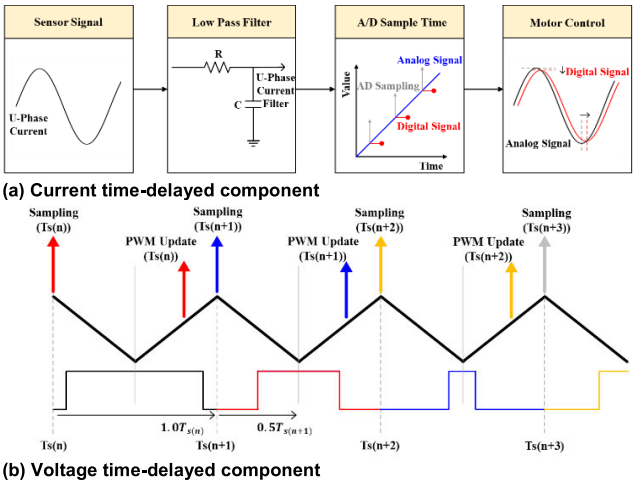

FIGURE 3. Current and voltage delay components.

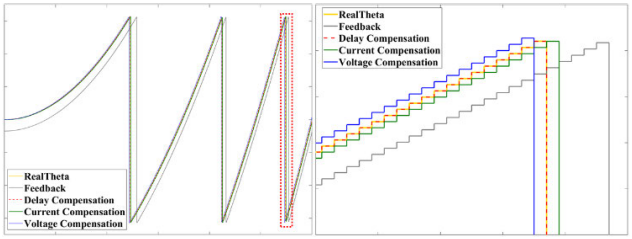

FIGURE 4. Comparison of electrical angles for current, voltage, and position time delays at high speeds.

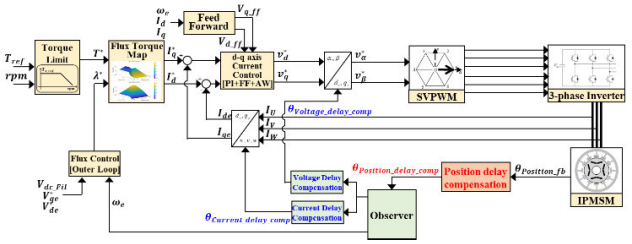

FIGURE 5. Torque control block diagram with delayed component compensation.

III. ANALYSIS OF PMSM CONTROL WITH ELECTRICAL ANGLE DELAYED COMPONENT COMPENSATION

A. SIMULATION SETUP

This study presents a method for detecting and compensating electrical angle delayed components to accurately determine the rotor position.

The delayed component error in inverter design can be detected using no-load speed control and a dynamo system. Friction and inertia consume current in no-load speed control. The amount of current consumed increases when the rotor position is not accurately compensated, thus leading to errors in the rotor position detection algorithm. The initial rotor position and delayed components can be compensated for by repeating the proposed method three or four times, thus allowing for estimating the accurate position. The detection

method using the dynamo system measures the d-q axis voltage by controlling the d-q axis current to 0 A at forward speed; this process is repeated in reverse rotation. Speed should be increased to minimize dead time and switching loss and increase the d-q axis voltage reliability.

TABLE 1. Simulation specification of the 15 kW traction motor.

Property	15 kW
Phase resistance [Ω]	0.0272
d-axis inductance [mH]	1.35
q-axis inductance [mH]	2.13
Magnetic flux [mVs/rad]	90.83
Poles	8
Position Delay [μs]	10
Position Offset [rad]	0.349

Table 1 presents resources from MATLAB Simulink, comparing the rotor position estimation through the unidirectional driving method of the preliminary study and the proposed delayed component detection and compensation method.

B. COMPARISON OF THE SIMULATION RESULTS

Fig. 6 shows graphs where the initial rotor position is detected using the unidirectional driving method (existing method) through MATLAB Simulink. As shown in Figs. 6(a) and 6(c), the initial rotor position is subject to errors due to delayed components as speed increases. Table 2 presents that the maximum error of the initial rotor position was 0.125 rad. In Figs. 6(b) and 7(d), the d-axis voltage decreased by compensating for the initial rotor position measured at 1000 rpm and measuring the d-q axis voltage using speed.

Thus, the detected initial rotor position at the measured speed included delayed components, thus resulting in position errors. The error rate increased with speed. In addition, the initial rotor position differed with the rotation direction. However, the rotor position error was the same for both forward and reverse rotations, indicating the influence of the delayed component $t_d\omega_e$.

As shown in Fig. 7(a), the proposed method matches the initial position of the rotor at different speeds. Although errors occurred owing to inaccurate voltages caused by losses at 1000 rpm, the initial rotor position matched at speeds over 2000 rpm. Fig. 7(b) shows data obtained by detecting delayed components, where a delayed component of 9.96 μs was detected at speeds above 2000 rpm. Forward and reverse d-axis voltages barely occurred by compensating for the detected initial rotor position and delayed components and measuring the d-q axis voltage, as shown in Figs. 8(a) and 8(b), and the forward and reverse q-axis voltages were symmetrical.

Therefore, the initial rotor position and position delay can be estimated accurately by detecting and compensating for delayed components.

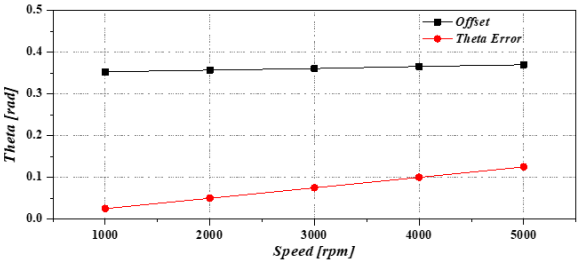

(a) Initial rotor position and error of the unidirectional driving method by speed [CCW]

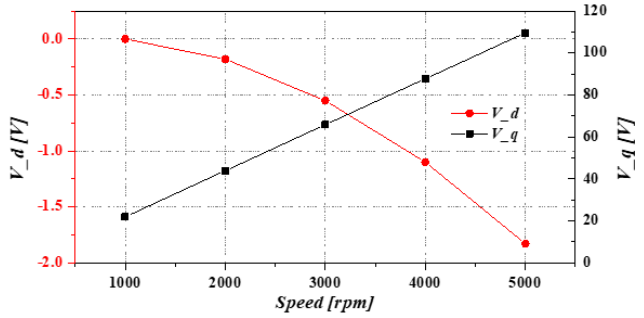

(b) d-q axis voltage of the unidirectional driving method by speed [CCW]

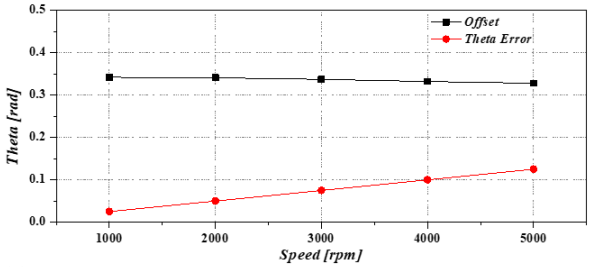

(c) Initial rotor position and error of the unidirectional driving method by speed [CW]

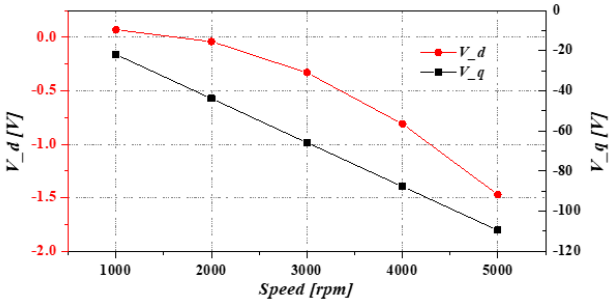

(d) d-q axis voltage of the unidirectional driving method by speed [CW]

FIGURE 6. Comparison of rotor initial position and d-q axis voltage of the unidirectional driving method by speed.

TABLE 2. Initial rotor position and position error by speed.

RPM	Theta offset [rad] (CCW/CW)	Theta error [rad] (CCW/CW)
1000	0.353/0.342	0.0042/0.0042
2000	0.357/0.341	0.0084/0.0084
3000	0.361/0.337	0.0126/0.0126
4000	0.366/0.332	0.0168/0.0168
5000	0.370/0.328	0.0209/0.0209

Fig. 9 shows the forward speed-dependent torque performance curves and torque control precision using the

TABLE 3. Initial rotor position, position error, and delayed components of delayed component compensation method at different speeds.

RPM	Theta offset [rad]	Theta error [rad]	Theta delay [μs]
1000	0.347	0.002	13.9
2000	0.348	0.001	9.97
3000	0.349	0.0	9.96
4000	0.349	0.0	9.95
5000	0.349	0.0	9.97

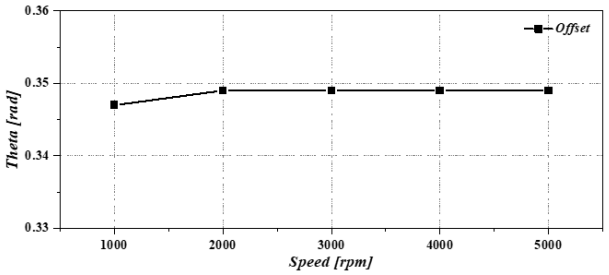

(a) Initial rotor position of delayed component compensation method by speed

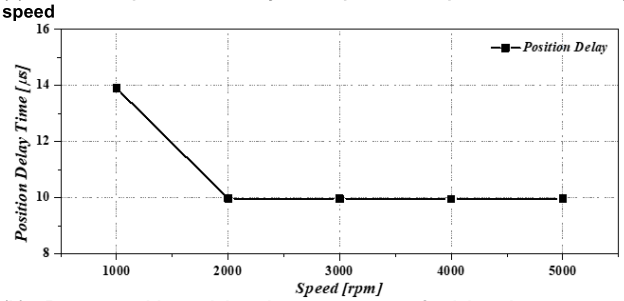

(b) Rotor position delayed component of delayed component compensation method by speed

FIGURE 7. Initial rotor position and position delayed component of delayed component compensation method at different speeds.

unidirectional driving (existing method) and proposed delayed component compensation methods. In the motoring section, the unidirectional driving method demonstrated a reduced feedback torque compared with the command torque with increased speed and an increased error rate, as shown in Figs. 9(a) and 9(c). Similarly, in the generating section, the feedback torque decreased compared with the command torque as speed increased, and the error rate increased, as shown in Figs. 9(b) and 9(d). By contrast, the proposed delayed component compensation method maintained almost constant command and feedback torques in the motoring and generating sections and exhibited an excellent precision of 1.67%.

Fig. 10 shows the reverse speed-dependent torque performance curves and torque control precision using the unidirectional driving (existing method) and the proposed delayed component compensation methods. The unidirectional driving method demonstrated an increased feedback torque compared with the command torque with increased speed in the motoring section and an increased error rate, as shown in Figs. 10(a) and 10(c). Similarly, in the generating

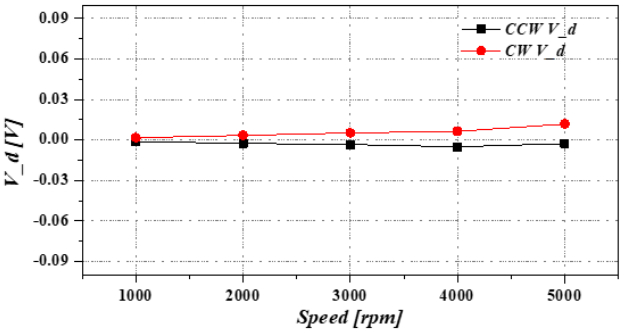

(a) d-axis voltage of delayed component compensation method by speed

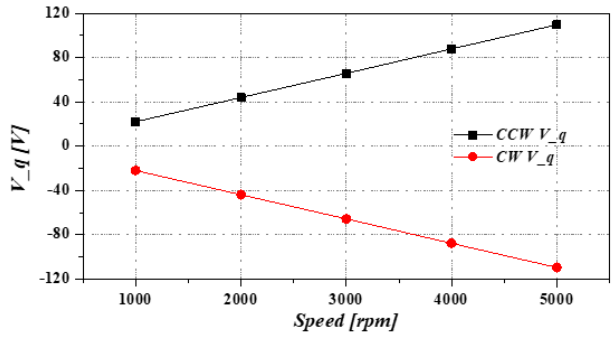

(b) q-axis voltage of delayed component compensation method by speed

FIGURE 8. Comparison of d-q axis voltage of delayed component compensation method at different speeds.

section, the feedback torque increased more than the command torque as the speed increased, and the error rate increased, as shown in Figs. 10(b) and 10(d). By contrast, the proposed delayed component compensation method maintained almost constant command and feedback torques in the motoring and generating sections and exhibited an excellent precision of 2.26%.

In conclusion, the unidirectional driving method increased torque error in the counterclockwise direction owing to an inaccurate rotor position caused by a 10μs delayed component. However, the delayed component compensation method compensated the 9.96μs delayed component, thus ensuring accurate initial rotor position and position delay and improving torque control performance.

IV. EXPERIMENT RESULTS OF PMSM CONTROL WITH ELECTRICAL ANGLE DELAYED COMPONENT COMPENSATION

A. EXPERIMENTAL SETUP

This section compares the existing unidirectional driving initial position and proposed delayed component compensation initial position detection methods. Further, the torque control performances are compared using position delay compensation during driving. The experiment was performed using a 15-kW traction motor and 90-kW towing motor (load motor of the dynamo system), as shown in Fig. 12. The 15-kW traction motor is an embedded PMSM using a resolver as the position sensor. Tables 4 and 5 present the motor and inverter specifications.

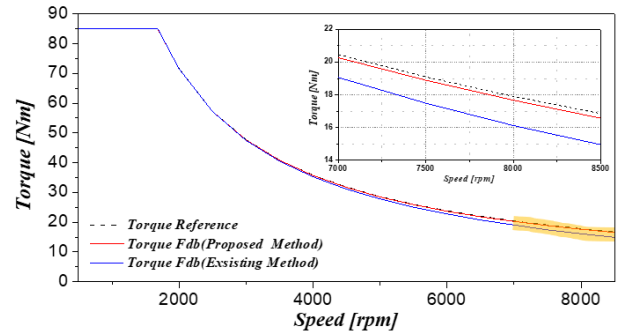

(a) Comparison of motoring torque control performance through the unidirectional driving method and delayed component compensation method [CCW]

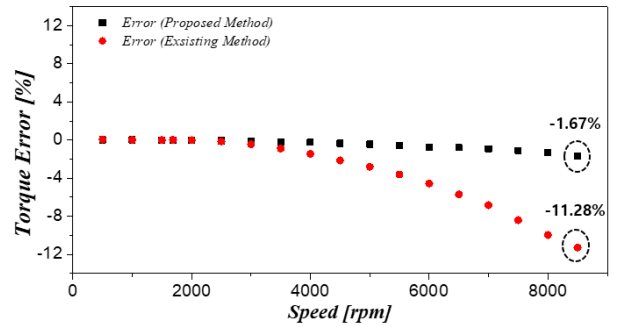

(b) Comparison of motoring torque control precision through the unidirectional driving method and delayed component compensation method [CCW]

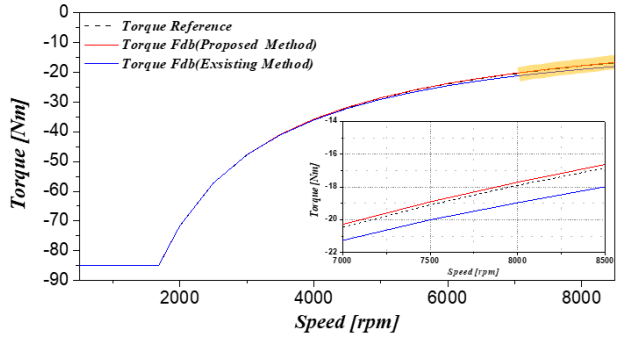

(c) Comparison of generating torque control performance through the unidirectional driving method and delayed component compensation method [CCW]

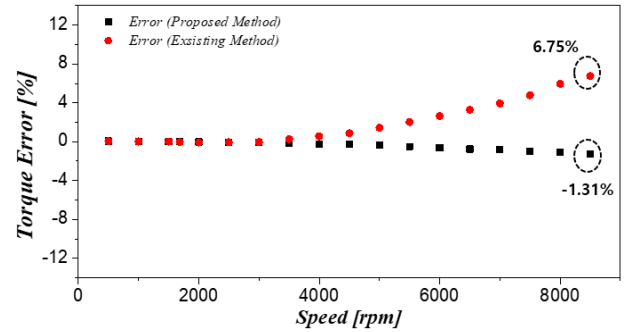

(d) Comparison of generating torque control precision through the unidirectional driving method and delayed component compensation method [CCW]

FIGURE 9. Comparison of motoring and generating torque control performance [CCW].

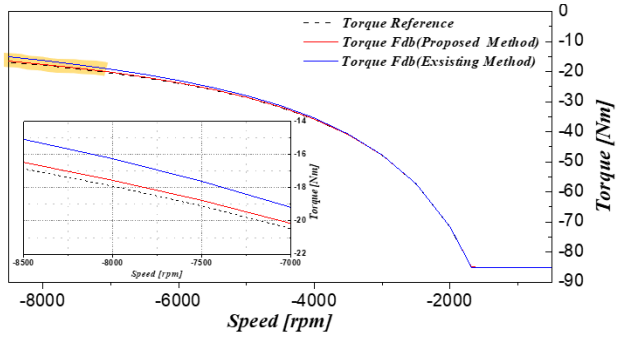

(a) Motoring torque control performance through the unidirectional driving method and delayed component compensation method [CW]

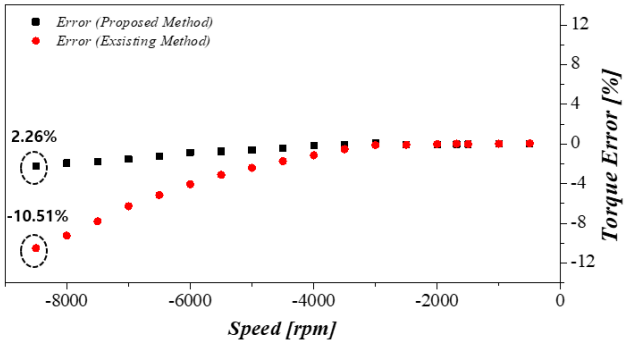

(b) Motoring torque control precision through unidirectional driving method and delayed component compensation method [CW]

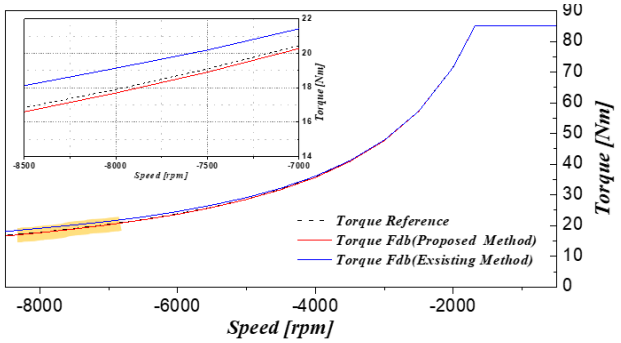

(c) Generating torque control performance through the unidirectional driving method and delayed component compensation method [CW]

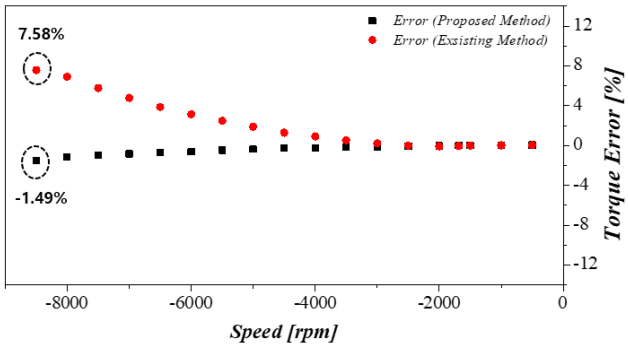

(d) Reverse generating torque control precision through unidirectional driving method and delayed component compensation method [CW]

FIGURE 10. Comparison of motoring and generating torque control performance [CW].

In this experiment, we controlled the d-q axis current to 0 A and measured the d-q voltage at each speed. We detected the delayed component and compensated for the detected delayed component using the proposed algorithm to detect

TABLE 4. Specification of the 15-kW traction motor.

Property	15 kW
Phase resistance [Ω]	0.0272
d-axis inductance [mH]	1.35
q-axis inductance [mH]	2.13
Magnetic flux [mVs/rad]	90.83
Poles	8

TABLE 5. Specification of the 15-kW inverter.

Property	15 kW
DC voltage [V]	320
Switching frequency [kHz]	4
Cooling type	Water Cooling

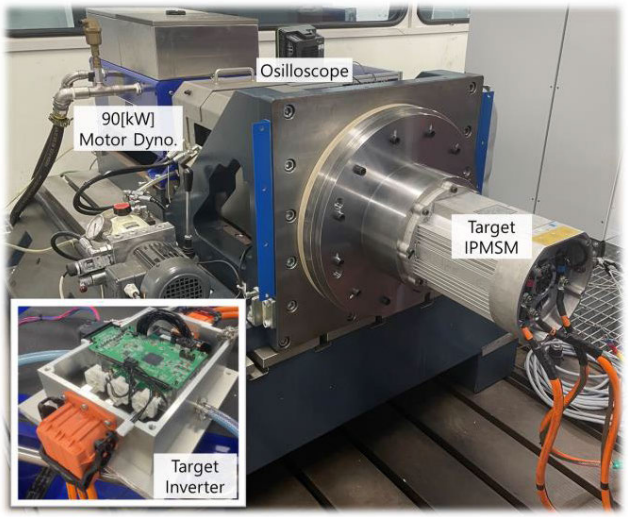

FIGURE 11. Motor dynamo test environment.

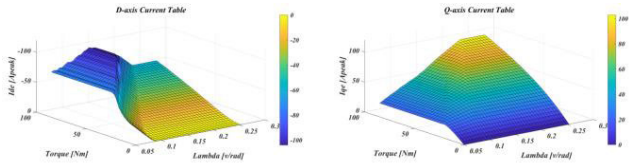

FIGURE 12. Flux-based current map table.

the rotor position. We used the flux-based current map in Fig. 12 rather than a speed–current map to validate the impact of delayed components and compare torque control performance.

B. COMPARISON OF THE EXPERIMENT RESULTS

First, we estimated the initial rotor position using the unidirectional driving method and verified the motor performance by applying the estimated initial rotor position. Subsequently, we verified the motor performance by applying the initial rotor position and position delay obtained through the proposed delayed component compensation method. Finally, we modified the resolver signal filter time constant, detected and compensated for delayed components, and verified the motor performance.

TABLE 6. Average initial rotor position and position error by the speed of the unidirectional driving method.

RPM	Theta offset [rad] (CCW)	Theta offset [rad] (CW)
500	0.607	0.597
1000	0.608	0.596
1500	0.611	0.593
2000	0.615	0.589
2500	0.619	0.585
3000	0.622	0.583
3500	0.624	0.580
4000	0.625	0.577

Table 6 presents the average data of the initial rotor position of the unidirectional driving method. The experiment was repeated five times, detecting the initial rotor position in 500 rpm increments up to 4000 rpm. As verified in the simulation, the initial rotor position increased in the forward direction and decreased in the reverse direction with increased speed. The initial rotor positions detected at 500 rpm were 0.607 rad [CCW] and 0.597 rad [CW]. Moreover, the initial position error by speed was proportional to $t_d\omega_e$. The d-axis voltage increased when the initial rotor position of 0.607 rad was applied, and the d-q axis voltage was measured, as shown in Fig. 13. The count in Figure (a) and (c) refers to the number of tests for each speed to find the initial position, and is the result of a total of 5 repeated tests.

Therefore, the unidirectional driving method inaccurately detected the initial rotor position owing to delayed components, thus rendering difficulty in determining a reliable speed range for the initial rotor position. Furthermore, the four-quadrant torque control performance decreased because the tendency of the initial rotor position error was opposite the rotation direction.

Fig. 14 shows the graphs of the detected initial rotor position and d-q axis voltage by applying the delayed component compensation method. The count in Figure (a) and (b) refers to the number of tests for each speed to find the initial position, and is the result of a total of 5 repeated tests. Table 7 presents the average data of the initial rotor position and delayed component. The experiment was repeated five times, detecting the initial rotor position in 500 rpm increments up to 4000 rpm. Almost no difference in the initial rotor position error by speed was observed. A considerable error can occur in the delayed component owing to minor changes in the voltage measured at 500 rpm because the delayed component value was extremely small. Thus, ensuring sufficient voltage can increase reliability. In the experiment, data measured from 1000 rpm and above exhibited high accuracy.

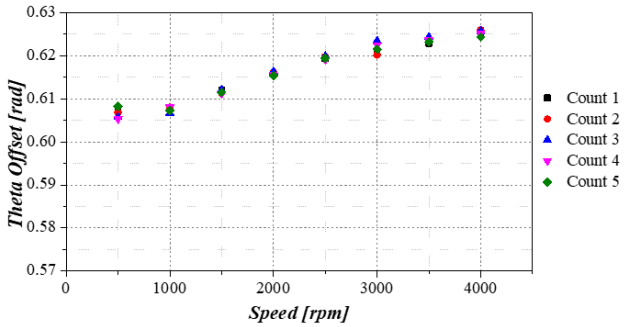

(a) Initial rotor position of the unidirectional driving method by speed [CCW]

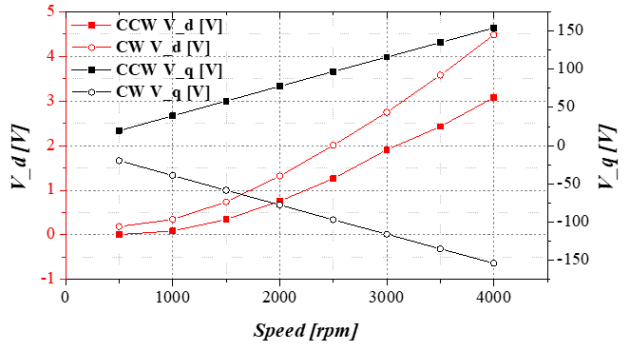

(b) d-q axis voltage of the unidirectional driving method by speed [CCW]

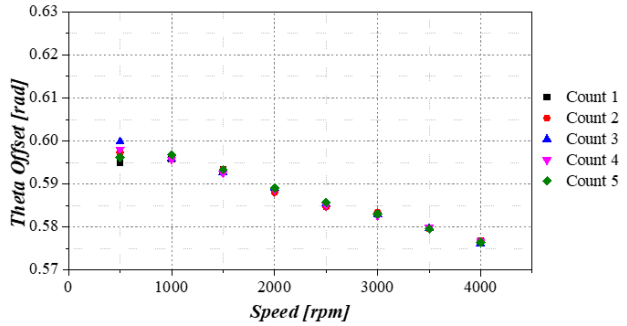

(c) Initial rotor position of the unidirectional driving method by speed [CW]

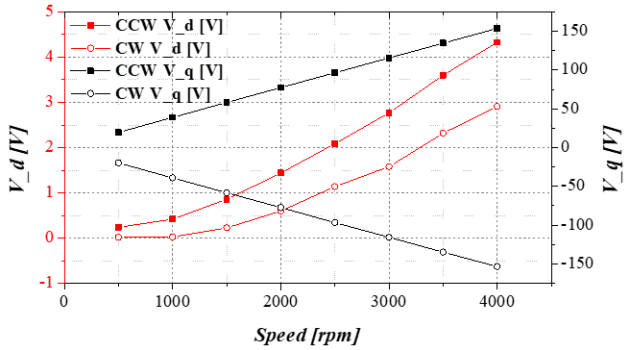

(d) d-q axis voltage of unidirectional driving method by speed [CW]

FIGURE 13. Comparison of rotor initial position and d-q axis voltage of the unidirectional driving method by speed.

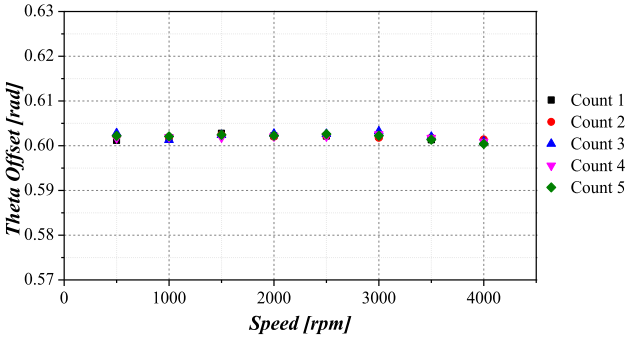

(a) Initial rotor position of delay compensation method by speed

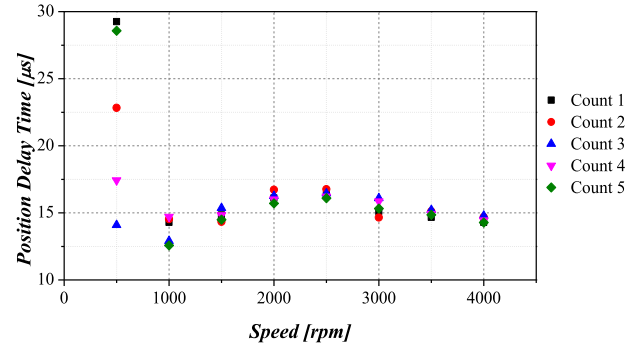

(b) Delayed component of delay compensation method by speed

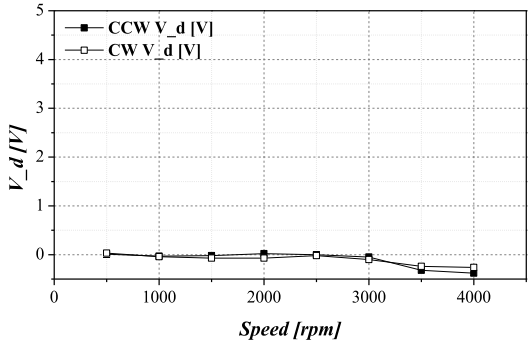

(c) d-axis voltage of delayed component compensation method by speed

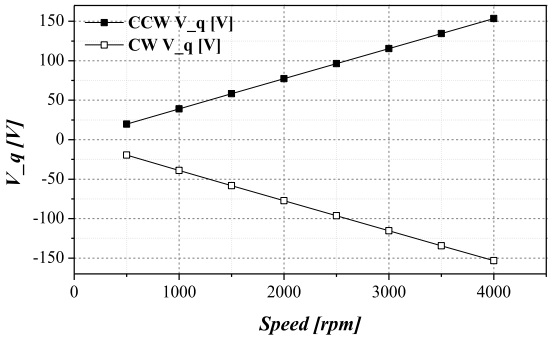

(d) q-axis voltage of delayed component compensation method by speed

FIGURE 14. Comparison of rotor initial position and d-q axis voltage of the unidirectional driving method by speed.

The torque control performance was compared by compensating 0.607 rad measured using the unidirectional driving method, along with 0.602 rad and a delayed component of 16.3 μs using the delayed component compensation method.

Fig. 15 shows the precision of four-quadrant torque control through delayed component compensation. The torque

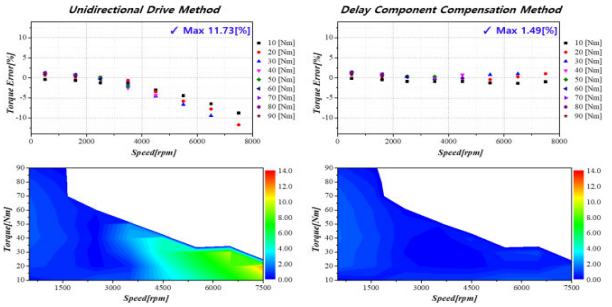

(a) Comparison of torque control precision in Quadrant 1

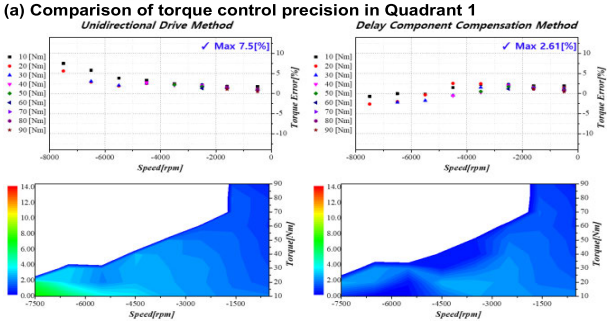

(b) Comparison of torque control precision in Quadrant 2

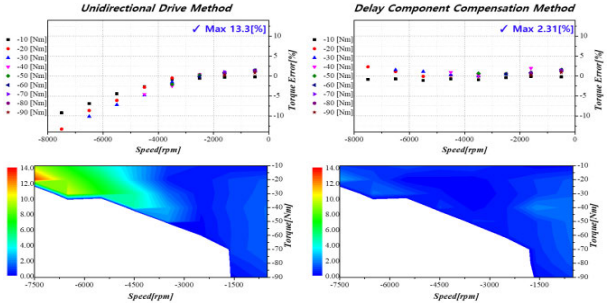

(c) Comparison of torque control precision in Quadrant 3

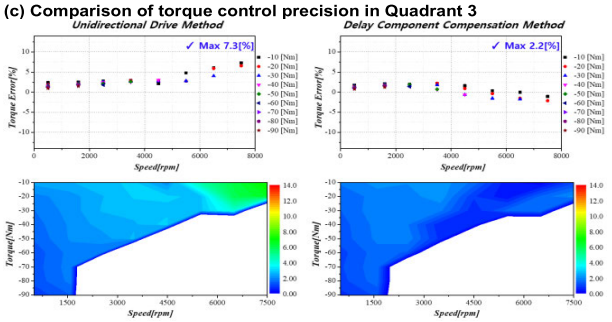

(d) Comparison of torque control precision in Quadrant 4

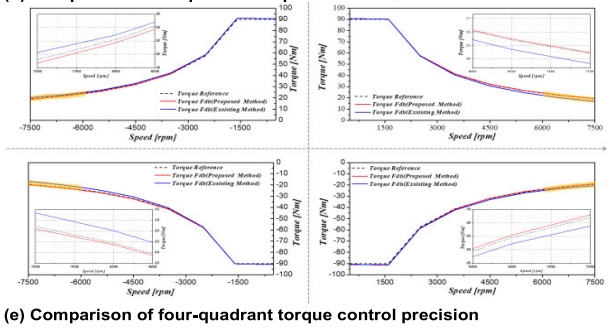

(e) Comparison of four-quadrant torque control precision

FIGURE 15. Comparison of four-quadrant torque control precision through delayed component compensation.

error rate increased sharply with increased speed for the unidirectional driving method. The proposed method had an

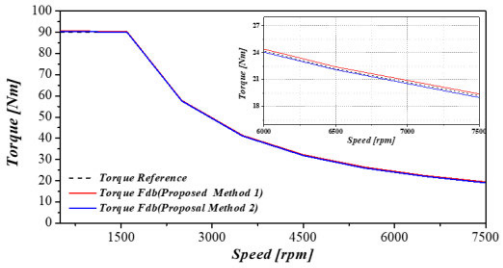

(a) Comparison of motoring torque control performance

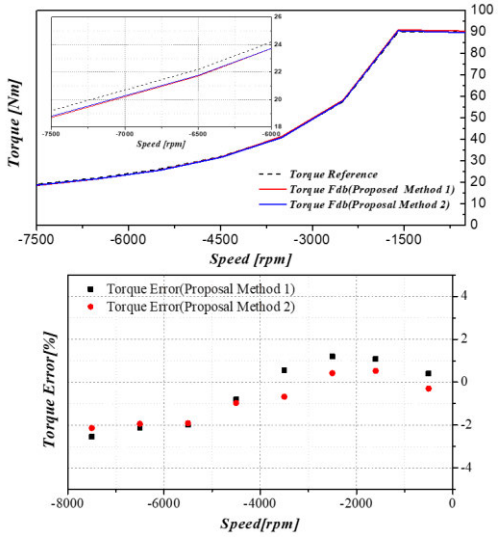

(b) Comparison of generation torque control performance

FIGURE 16. Comparison of torque control performance by change in filter time constant.

extremely small error rate with increased speed. Furthermore, the unidirectional driving method exhibited torque tilting in the counterclockwise direction during four-quadrant driving owing to delayed components. Unlike the unidirectional driving method, the proposed method maintained an almost constant torque. It yielded excellent torque control precision, with a maximum of 13.3% and 2.61% for the unidirectional driving and proposed methods, respectively.

Table 8 presents the delayed component measurement data, which compares the delayed components when the filter cutoff frequency of the sin and cos signals of the revolver was modified from 32.3 to 9.0 kHz. Circuit filter, peripheral, and algorithm delays were delayed components measured using an oscilloscope, and detection delay was the delayed component detected through the proposed algorithm. Converted into detected data, the difficult-to-detect hardware delay was -14.2 and -16 μs, a small error rate to be reliable.

TABLE 7. Average initial rotor position and delayed component by speed for the delayed component compensation method.

RPM	Theta offset[rad]	Delayed component [μs]
500	0.602	22.4
1000	0.602	13.8
1500	0.602	14.8
2000	0.602	16.1
2500	0.602	16.3
3000	0.602	15.4
3500	0.602	15.0
4000	0.601	14.5

TABLE 8. Delayed component measurement data.

RPM	Proposal Method1 (fc: 32.3 kHz)	Proposal Method2 (fc: 9.0 kHz)
Hardware delay [μs]	−14.2	−16
Circuit filter delay [μs]	6.5	15
Peripheral delay [μs]	−0.9	−0.9
Algorithm delay [μs]	−7.7	−7.7
Detection delay [μs]	−16.3	−9.6

Detecting and compensating the delayed components using Proposal Method1 and Proposal Method2 demonstrated a torque error rate of less than 2% between motoring and generation, as shown in Fig. 16. Even if the inverter design changes the delayed component, the torque control performance can be maintained by compensating the delayed component using the proposed algorithm.

V. CONCLUSION

This study analyzed electrical angle delayed components caused by inverter components and design errors and compared the existing rotor position detection method to assess the impact of electrical angle delayed components. An algorithm for detecting and compensating for the delayed components was proposed and experimentally validated to accurately detect the rotor position. The unidirectional driving method was used as a reference, which is easy to compare and analyze for delayed component detection and predominantly used in PMSM mass production.

The proposed detection of the rotor position by compensating for electrical angle delayed components was classified into an analysis of the initial rotor and time-delay position detections. The delayed component was detected and compensated for in the initial rotor position detection to accurately detect the initial rotor position. The time-delay position detection proposed and compensated for new position, current, and voltage time delays through delayed component compensation to accurately detect the rotor position.

For the initial rotor position detection, under the unidirectional driving method, the delayed component t_d was proportionate to ω_e, resulting in a maximum occurrence of 0.2 rad. The maximum error was 0.048 rad, with 0.625 and 0.577 rad in the forward and reverse directions, respectively, by the error of $\frac{\Delta\theta}{2}$ according to the rotation direction. By contrast, the proposed method detected a delayed component of -16.3 μs and compensated for it with the d-q axis equation, resulting in an initial rotor position error of 0.001 rad according to speed. No initial position errors occurred in either the forward or reverse direction. A maximum error of 4.0% was observed when comparing the initial position error of 0.625 rad in the unidirectional driving method with the 0.601 rad of the proposed method.

The time-delay position was analyzed for torque control precision using a flux-based current map. The unidirectional driving method exhibited an increased torque error rate with speed, and the maximum torque control precision was 13.3%. The proposed method was highly resilient to speed increase and achieved a 2.6% torque control precision.

In addition, even when the delayed component filter time constant was changed from 32.3 kHz to 9.0 kHz, the proposed algorithm maintained the torque control performance within 2%.

Finally, the electrical angle delayed component varied with the inverter components and design errors. This study is significant for improving torque control performance by robustly and accurately detecting the rotor position against inverter components and design errors through the delayed component detection and compensation method.

REFERENCES

[1] G. Boztas and O. Aydogmus, "Design of a high-speed PMSM for flywheel systems," in *Proc. 4th Int. Conf. Power Electron. Appl. (ICPEA)*, Sep. 2019, pp. 1–5.

[2] N. Murali and S. Ushakumari, "Performance comparison between different rotor configurations of PMSM for EV application," in *Proc. IEEE REGION 10 Conf. (TENCON)*, Nov. 2020, pp. 1334–1339.

[3] G. Pellegrino, A. Vagati, P. Guglielmi, and B. Boazzo, "Performance comparison between surface-mounted and interior PM motor drives for electric vehicle application," *IEEE Trans. Ind. Electron.*, vol. 59, no. 2, pp. 803–811, Feb. 2012.

[4] D. D. Popa, L. M. Kreindler, R. Giuclea, and A. Sarca, "A novel method for PM synchronous machine rotor position detection," in *Proc. Eur. Conf. Power Electron. Appl.*, 2007, pp. 1–10.

[5] S. Sakunthala, R. Kiranmayi, and P. N. Mandadi, "A study on industrial motor drives: Comparison and applications of PMSM and BLDC motor drives," in *Proc. Int. Conf. Energy, Commun., Data Anal. Soft Comput. (ICECDS)*, Aug. 2017, pp. 537–540.

[6] S. Bai and E. W. Zhang, "Based on the model of the DQ axis permanent magnet synchronous motor MPC," in *Proc. Int. Conf. Electron. Optoelectron.*, vol. 3, Jul. 2011, pp. V3-224–V3-226.

[7] T. Wu, D. Luo, S. Huang, X. Wu, K. Liu, K. Lu, and X. Peng, "A fast estimation of initial rotor position for low-speed free-running IPMSM," *IEEE Trans. Power Electron.*, vol. 35, no. 7, pp. 7664–7673, Jul. 2020.

[8] D. Lu, J. Gu, J. Li, M. Ouyang, and Y. Ma, "High-performance control of PMSM based on a new forecast algorithm with only low-resolution position sensor," in *Proc. IEEE Vehicle Power Propuls. Conf.*, Sep. 2009, pp. 1440–1444.

[9] C. W. Secrest, J. S. Pointer, M. R. Buehner, and R. D. Lorenz, "Improving position sensor accuracy through spatial harmonic decoupling, and sensor scaling, offset, and orthogonality correction using self-commissioning MRAS methods," *IEEE Trans. Ind. Appl.*, vol. 51, no. 6, pp. 4492–4504, Nov. 2015.

[10] K.-Y. Cho, Y.-K. Lee, H.-S. Mok, H.-W. Kim, B.-H. Jun, and Y.-H. Cho, "Torque ripple reduction of a PM synchronous motor for electric power steering using a low resolution position sensor," *J. Power Electron.*, vol. 10, no. 6, pp. 709–716, Nov. 2010.
[11] D. C. Hanselman, "Resolver signal requirements for high accuracy resolver to digital conversion," *IEEE Trans. Ind. Electron.*, vol. 37, no. 6, pp. 556–561, Dec. 1990.
[12] D. C. Hanselman, "Technique for improving resolver-to-digital conversion accuracy," *IEEE Trans. Ind. Electron.*, vol. 38, no. 6, pp. 501–504, Dec. 1991.
[13] A. Bunte and S. Beineke, "High-performance speed measurement by suppression of systematic resolver and encoder errors," *IEEE Trans. Ind. Electron.*, vol. 51, no. 1, pp. 49–53, Feb. 2004.
[14] S. S. Kuruppu, S. G. Abeyratne, and S. Hettiarachchi, "Modeling and detection of dynamic position sensor offset error in PMSM drives," *IEEE Access*, vol. 11, pp. 36741–36752, 2023.
[15] S. S. Kuruppu and Y. Zou, "Static position sensor bias fault diagnosis in permanent magnet synchronous machines via current estimation," *IEEE/ASME Trans. Mechatronics*, vol. 26, no. 2, pp. 888–896, Apr. 2021.
[16] M. Konghirun, "Effects and detection of misaligned position sensor in AC servo drive system with filtered current delay," in *Proc. Int. Conf. Electr. Mach. Syst.*, 2008, pp. 978–983.
[17] A. K. Singh, R. Raja, T. Sebastian, and A. Gebregergis, "Effect of position measurement delay on the performance of PMSM drive," in *Proc. IEEE Energy Convers. Congr. Expo. (ECCE)*, Sep. 2018, pp. 4622–4627.
[18] J. S. Bang and T. S. Kim, "Automatic calibration of a resolver offset of permanent magnet synchronous motors for hybrid electric vehicles," in *Proc. Amer. Control Conf. (ACC)*, Jul. 2015, pp. 4174–4179.
[19] J.-Y. Park, Y.-K. Ko, D.-Y. Jang, M.-S. Kwak, and Y.-K. Lee, "Auto calibration of position sensor while driving ECO vehicle," in *Proc. IEEE Transp. Electrific. Conf. Expo, Asia–Pacific*, Jun. 2016, pp. 397–401.
[20] L. M. Gong and Z. Q. Zhu, "Robust initial rotor position estimation of permanent-magnet brushless AC machines with carrier-signal-injection-based sensorless control," *IEEE Trans. Ind. Appl.*, vol. 49, no. 6, pp. 2602–2609, Nov. 2013.
[21] S. Medjmadj, D. Diallo, C. Delpha, and G. Yao, "A salient-pole PMSM position and speed estimation at standstill and low speed by a simplified HF injection method," in *Proc. 43rd Annu. Conf. IEEE Ind. Electron. Soc.*, Oct. 2017, pp. 8317–8322.
[22] J. Liu, Y. Zhang, H. Yang, and W. Shen, "Position sensorless control of PMSM drives based on HF sinusoidal pulsating voltage injection," in *Proc. IEEE Energy Convers. Congr. Expo. (ECCE)*, Oct. 2020, pp. 3849–3853.
[23] B. Yuanjun, G. Xinhua, S. Xiaofeng, W. Yanfeng, and C. Yin, "Initial rotor position estimation of PMSM based on high frequency signal injection," in *Proc. IEEE Conf. Expo Transp. Electrific. Asia–Pacific*, Aug. 2014, pp. 1–4.
[24] D. Kim, J. Kim, H. Lim, J. Park, J. Han, and G. Lee, "A study on accurate initial rotor position offset detection for a permanent magnet synchronous motor under a no-load condition," *IEEE Access*, vol. 9, pp. 73662–73670, 2021.
[25] B.-H. Bae and S.-K. Sul, "A compensation method for time delay of full-digital synchronous frame current regulator of PWM AC driver," *IEEE Trans. Ind. Appl.*, vol. 39, no. 3, pp. 802–810, May 2003.
[26] S.-H. Song, J.-W. Choi, and S.-K. Sul, "Current measurements in digitally controlled AC drives," *IEEE Ind. Appl. Mag.*, vol. 6, no. 4, pp. 51–62, Jul. 2000.

SEONHYEONG KIM received the B.S. and M.S. degrees in automotive engineering from Kookmin University, Seoul, Republic of Korea, in 2014 and 2016, respectively, where he is currently pursuing the Ph.D. degree in automotive engineering. From 2016 to 2021, he was with the Hyundai Mobis Research and Development Division, e-PowerTrain Business Unit, where he developed an inverter system for automotive. He is also with the Korea Institute of Electronics Technology. His current research interests include electric vehicles and inverters.

KEUNHO PARK received the M.S. and Ph.D. degrees in electronic information engineering from Jeonbuk National University, Jeonju, Republic of Korea, in 2015 and 2019, respectively. Since 2021, he has been with the Korea Institute of Electronics Technology, where he was a Postdoctoral Lecturer, from 2019 to 2020. His current research interests include machine vision, artificial intelligence, and deep learning.

DONGKIL KANG received the B.S. degree in computer science from Ulsan University, Ulsan, South Korea, in 2015. He is currently pursuing the Ph.D. degree in automotive engineering with Kookmin University. His current research interests include the advanced control of electric machines and electric vehicles.

GEUN HO LEE received the B.S. and M.S. degrees in electrical engineering and the Ph.D. degree in automotive engineering from Hanyang University, Seoul, South Korea, in 1992, 1994, and 2010, respectively. From 1994 to 2002, he was with the LG Industrial Research Institute, where he developed inverter systems for elevators. Since 2011, he has been a Professor in automotive engineering with Kookmin University. His current research interests include electric vehicles and the advanced control of electric machines.